# Conceptual Design of the PANDA Magnet System

Evgeny K. Koshurnikov, Alexander A. Efremov, Yuri Yu. Lobanov, Alexander F. Makarov, Herbert Orth, Alexey N. Sissakian, and Alexandre S. Vodopianov

***Abstract*—A magnet system comprising a 2 T superconducting solenoid for a target spectrometer and a large aperture dipole magnet for a forward spectrometer is being developed for the PANDA experiment at GSI. The inner radius of the solenoid coil is 1.1 m. The solenoid is of a split type to provide a warm bore between the coil parts for the target. An energy of 23 MJ is stored in the magnet. The Dipole Magnet will provide a bending momentum of 2 T · m. The magnet is of the "H-type" with a water-cooled winding. The paper covers magnetic field and forces calculations as well as strength analysis and description of the magnet system components and their implementation.**

***Index Terms*—Dipole magnet, electromagnetic forces, spectrometry, superconducting solenoid.**

## I. Introduction

THE panda experimental facility at HESR (FAIR, GSI, Darmstadt, Germany) [1] will include a target spectrometer with a 2 T solenoid and a large aperture 2 T · m dipole magnet—an element of the forward spectrometer—that is downstream of the solenoid. The PANDA magnet system layout is shown in Fig. 1.

All central detectors are placed inside the superconducting solenoid coil. Thus the requirement of the radiation transparency has not been included in the specification for the materials of the solenoid coil. So, the design can differ from the traditional one for large detector solenoids with an aluminum stabilized superconductor implying an inner winding method [2], [3]. The solenoid is of a split type to ensure a warm hole of 100 mm in diameter between the unequal coil parts for the Cluster Target System mounting.

The Dipole Magnet of the PANDA Forward Spectrometer is of an "H-type" with a rectangular conical aperture and an Al water-cooled winding. The general view of the PANDA magnet system is shown in Fig. 2.

## II. Superconducting Solenoid

### A. Magnet Design

Fig. 3 shows the longitudinal cross section of the PANDA superconducting solenoid with the dimensions of the cryostat, the superconducting coil and the iron yoke indicated in it. The main parameters of the solenoid are given in Table I.

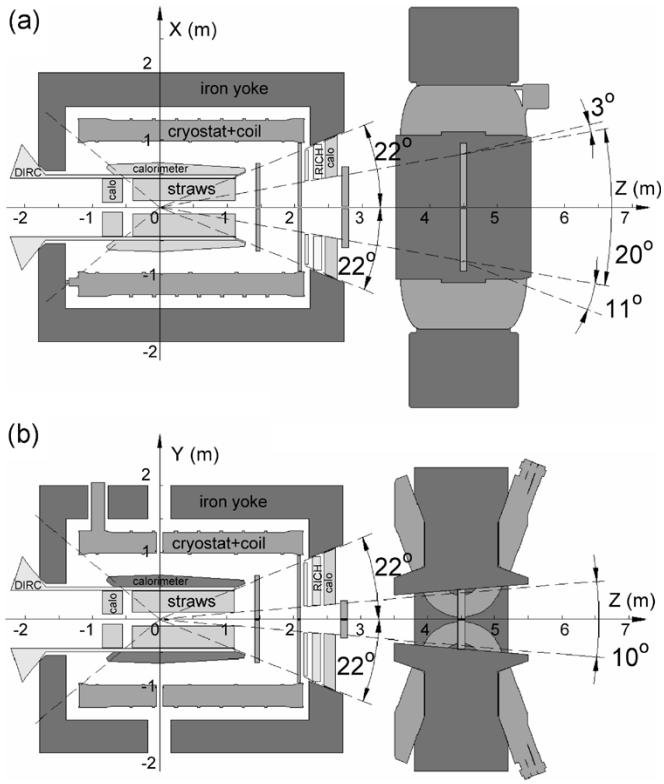


Fig. 1. PANDA magnet system layout. a) Top view, b) side view.

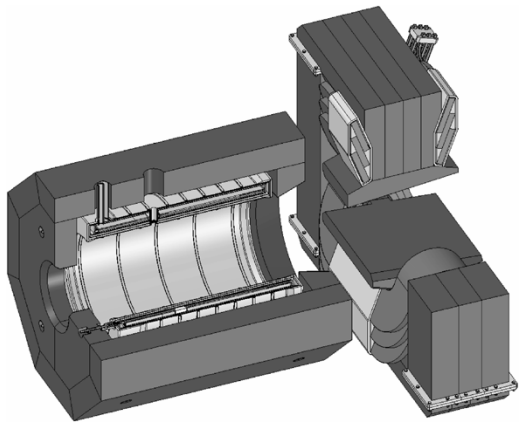

Fig. 2. 3D view of the PANDA magnet system.

The superconducting coil with an average current density of $5 \cdot 10^7$ A/m$^2$ was designed to achieve the required magnetic flux density of 2.0 T in the straw detector area.

An acceptable level of field inhomogeneity 1.55% in the straw detector area was achieved using correcting coils 3, 4 and 5 placed at the outer surface of the main coils. These coils compensate local magnetic field inhomogeneity resulting from splitting the solenoid and initial design constraints on the solenoid

Manuscript received September 20, 2005. This work was supported in part by INTAS under Grant 03-54-3710, andin part by Commission of European Communities under Grant "DIRAC secondary beams" 515873.

E. K. Koshurnikov, A. A. Efremov, Y. Y. Lobanov, A. F. Makarov, A. N. Sissakian, and A. S. Vodopianov are with the Joint Institute for Nuclear Research (JINR), Joliot-Curie 6, Dubna, 141980 Moscow Region, Russia (e-mail: root@magnet.spb.su).

H. Orth is with the Gesellschaft fur Schwerionenforshung mbH (GSI), Abtl. KP3, Planckstraße 1, D_64291 Darmstadt, Germany (e-mail: h.orth@gsi.de).

Digital Object Identifier 10.1109/TASC.2005.869643

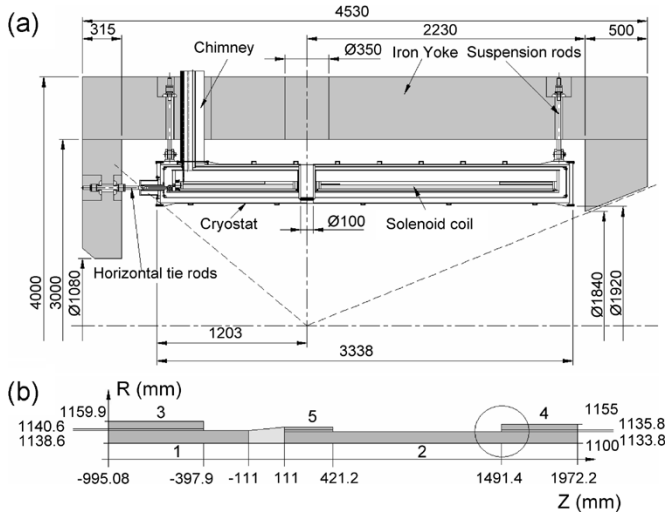


Fig. 3. SC solenoid. a) Solenoid longitudinal cross section, b) Coil dimensions.

TABLE I
MAIN PARAMETERS OF THE SOLENOID

| | |
|---|---|
| Axial component of the magnetic induction in the center of the solenoid, T | 2.04 |
| Ampere-turns of the solenoid, MA | 6.02 |
| Nominal operational current, A | 1880 |
| Design current density (without ground wall insulation), MA/m$^2$ | 50 |
| Stored energy, MJ | 23 |
| Self inductance, H | 13 |
| Maximum induction in the superconducting winding at operational current, T | 3.2 |

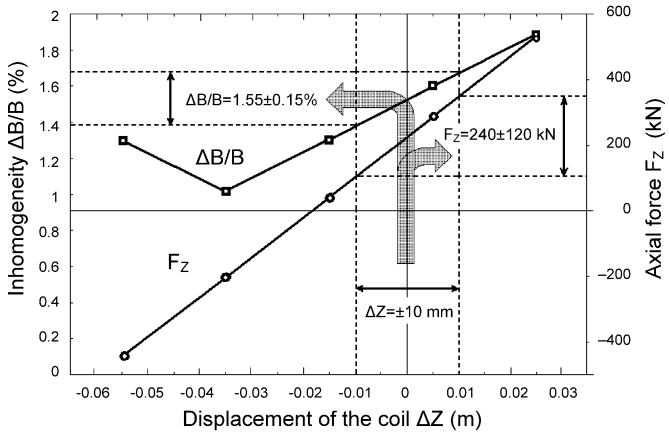


Fig. 4. Axial force Fz and field inhomogeneity $\Delta B/B$ in the operation area versus coil axial displacement $\Delta Z$.

length. The inhomogeneity dispersion $\pm 0.15\%$ corresponds to axial tolerance of the coil positioning $\pm 1$ cm with respect to the yoke (Fig. 4).

Simulations with TOSCA were performed to calculate magnetic fields and forces acting on the solenoid coils and on the iron yoke. The peak induction in the coil area is 3.2 T. The stray field at a radial distance of 4 m from the magnet system (solenoid + dipole) does not exceed 3 mT. The stray field in the photo multiplier tubes (PMT) area of the Cherenkov detector (DIRC)

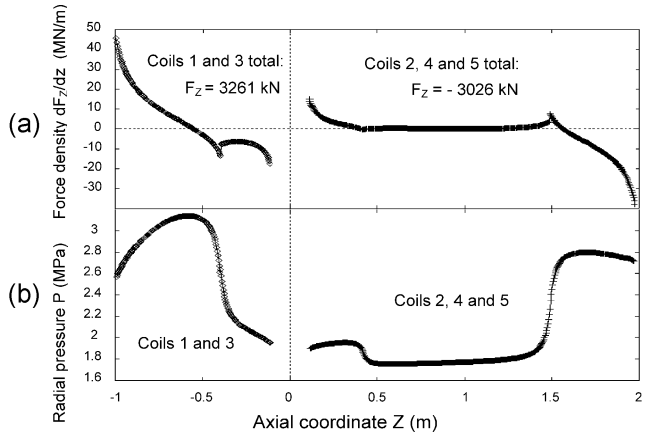


Fig. 5. Distribution of the axial force density and radial pressure.

TABLE II
PARAMETERS OF THE SUPERCONDUCTING CABLE

| | |
|---|---|
| **C-form chanel** | |
| Material | Cu (RRR 100) |
| Overall dimensions, mm$^2$ | $4 \times 7$ |
| Groove for flat cable, mm$^2$ | $1.22 \times 3.62$ |
| **SC insert** | |
| Material | NbTi/Cu |
| Cu/NbTi ratio | 1.3/1 |
| Critical current (B= 3.3T, T=4.2K), A | 4598 |
| Number of filaments | 54 |
| Filament diameter, μm | 54 |

(see Fig. 1) does not exceed 10 mT (PMT's are placed at the upstream end of DIRC). Axial forces acting on the solenoid coil and the field inhomogeneity in the straw detector area versus the coil displacement in axial direction are shown in Fig. 4.

If the solenoid coil is inclined at an angle of 1° from the axis Z, a torque of 3.5 $\mathrm{kN} \cdot \mathrm{m}$ is applied to the coil. A radial displacement of the coil by 1 cm with respect to the yoke produces a radial offset force of 32 kN. Distribution of the radial pressure and the axial force density characterizing concentration of the axial magnetic force along the coil axis are shown in Fig. 5. The axial attraction force between both parts of the coil is about 3100 kN. The maximum radial pressure on the inner surface of the coil is about 3.2 MPa.

### *B. Conductor Design*

The conductor consists of a superconductor flat Rutherford cable soldered in a high purity copper C-form beam profile 4 mm $\times$ 7 mm The operational current is 1880 A that is essentially smaller than the current of 5 kA (or higher) in large detector magnets with the same magnetic induction 2 T in the central area [2], [3]. The flat cable is braided of 11 superconducting strands 0.6 mm in diameter which have 54 superconducting filaments of a diameter 54 $\mu\mathrm{m}$. The Cu:SC ratio is 1.3. The main design parameters of the copper matrix and the superconducting cable are summarized in Table II.

### *C. Coil Structural Layouts*

The general structural layout of the coreless solenoid coil is shown in Fig. 6. Shear stresses at the boundary coil-mandrel are minimized by separating the whole winding body from the

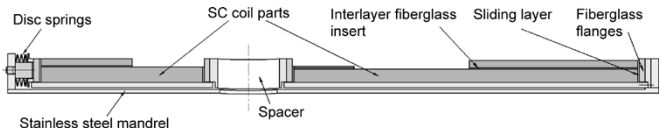


Fig. 6. PANDA magnet system layout.

coil former. It provides the natural shape of the coil as the solenoid is energized. The coil is wound on an Al alloy tube. This method of winding is simpler than the inner winding method used for manufacturing large detector solenoids with aluminum stabilized conductor. The Al tube is used as a secondary dump turn for quench protection as well. A prepreg interlayer cloth is deposited between the coil layers during winding. After the winding is completed the coil is heat treated to cure the epoxy. To prevent gluing of the coil surface to the Al tube a release coating is applied at the tube surface before winding. A guaranteed gap between the coil inner surface and the mandrel outer surface has to be created after cooling down the magnet. The coil shrinks during the cooling down. Additionally it shortens because of the compressive axial electromagnetic forces. A set of disk springs fixing spatial position of the coil is distributed along the coil flange circle. Changes of the coil length are compensated by these springs.

The hoop stress inside the coil is completely carried by the cable, unlike the detector coils with aluminum stabilized conductor.

The two coil parts are separated by the spacer for the target (Fig. 6). A precompression of 160 kN is applied to prevent separation of the coil parts at the contact surfaces coil-insert and coil-flanges under gravity when the coil is not energized.

The fiberglass flanges and the coil end face surfaces are separated by PTFE and kapton film layers in order to decrease friction under the cooling down and energizing.

### *D. Mechanical Analysis of the Solenoid Coil*

The deflected mode of the coil composite material was analyzed using a computer code COSMOS in the framework of the linear Finite-Element model of the coil. The electromagnetic loads were applied as nodal forces obtained from the corresponding local force densities calculated using TOSCA.

There are considerable shear stresses produced by temperature deformations and by axial magnetic forces at the correcting coil inner radius and inside the separating fiberglass spacer. Shear stresses generated by temperature deformations and temperature plus magnetic forces at the boundary of coil 2 and correcting coil 4 (see circled area in Fig. 3(b)) are shown in Fig. 7. It can be seen that the thickness of the fiberglass insert (Fig. 6) influences the maximum value of shear stresses. A thicker insert provides lower level of shear stresses.

### *E. Coil Supports and Fine Adjustment of the Coil Position*

The forces acting on the coil are its own weight (105 kN) and the axial magnetic force (240 kN). Sufficiently high axial offset force is required due to unidirectional action of axial ties and a

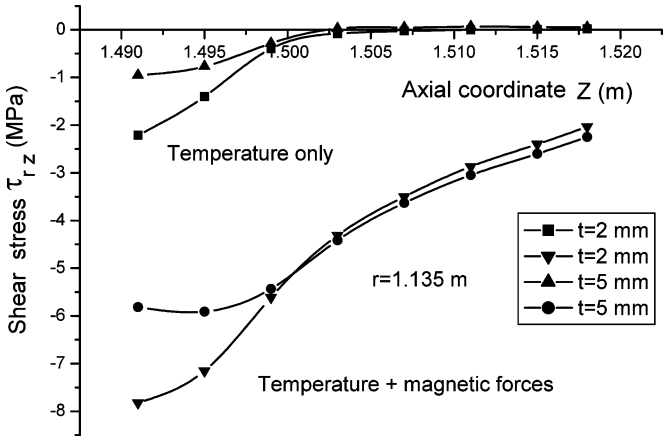


Fig. 7. Maximum shear stress as a function of thickness t of the fiberglass insert between main coil 2 and correcting coil 4.

considerable axial force gradient (120 kN/cm). The coil suspension system consists of twenty stainless steel supports (16 radial and 4 vertical rods) fixed at the ends of the outer vacuum shell. The axial magnetic force in the axis Z direction is carried by three stainless steel rods (Fig. 3(a)). The position of the coil has to be adjusted taking into account thermal shrinkage of the coil and the coil supports as well as the yielding of the support ties and a nonlinear dependence of the axial force on the solenoid current. A deviation of the axial force $\pm 120$ kN corresponds to a shift of the coil axial position $\pm 10$ mm that sets up strict requirements on the coil adjustment precision.

### *F. Protection System*

A quench protection system based on extracting energy from the series-connected subcoils (1–5) to an external dump resistor of 0.25 Ohm and to the Al supporting cylinder is chosen.

According to calculations, the hot spot temperature in the coil after the quench is $\sim$75 K, the temperature of the Al cylinder is $\sim$62 K. As an additional backup, the active heaters placed at the outer surface of the coil provide a quench back in the whole solenoid coil in the event of failure of the quench protection circuitry and thereby limit temperature gradients inside the coil composite material.

### *G. Cooling Mode and Thermal Design*

Helium bath cooling was chosen for the solenoid coil. That implies a closed helium volume ($\sim 1.2\,\mathrm{m}^3$).

Four low-heat-conduction vertical ties, 3 axial ties and 16 radial struts support the cold mass of the cryostat. The coil is surrounded by a thermal shield, which is supported from the side of the vacuum chamber and cooled by He gas (inlet temperature 60 K). Stainless steel foil 50 $\mu$m thick sputtered by high purity Al [4] is applied to reduce heat loads both on the shield and on the coil. A radiation load of 0.15 W has been evaluated for the cold volume. This value is obtained from a heat flux of $\sim 4.2\,\mathrm{mW/m}^2$ over $36\,\mathrm{m}^2$ of the solenoid surface covered with an aluminized stainless steel foil. The data of the heat load at the level 4.2 K multiplied by the safety factor 2 are summarized in Table III. An additional thermal load given by eddy currents in

TABLE III
HEAT LOADS ON THE COLD VOLUME

| | | |
|---|---|---|
| Radiation, W | | 0.3 |
| Support conduction, W | | 3.4 |
| Residual gas conduction, W | | 0.14 |
| Conductor joints and wires, W | | 2 |
| HTS current leads, W | | 0.9 |
| | ***Total:*** | 6.74 |

the cryostat shells occurs when the coil is ramping up or discharging. A time interval for energizing the coil which ensures an acceptable heat load is about 1 hour.

It is planned to use HTS current leads [5]. They are designed for conduction cooling and do not require helium flow cooling. Its conductive heat leak at 64 K–4.2 K per pair is only 0.45 W. The "warm" parts of the current leads (64 K–300 K) cooled by addition helium gas flow are optimized to provide minimum energy consumption at the level 64 K.

The overall heat load at the level 4.2 K is expected not to exceed 6.7 W in the operational mode and about 38 W in the transient mode. The overall heat load at the level 64 K is expected not to exceed 600 W in the operational mode and about 610 W during ramping.

### *H. Design of the Cryostat*

Stainless steel was chosen as the material of the cryostat to ensure mechanical stability of the cylindrical shells of the vacuum vessel and the cold volume. The ends of the shells are thickened to provide a means for anchoring the rods used to support the coil (Fig. 3). Both outer shells of the cryostat have stiffening ribs. The vacuum vessel has a chimney for the current leads, LHe and GHe inlets and outlets, the diagnostic wires and vacuum pumping as shown in Fig. 3(a).

### *I. Iron Yoke*

The yoke has an octagonal shape. It is closed by unequal end caps on both sides (see Fig. 3(a)). The total weight of the yoke is 2400 kN. The yoke is built of modules which are bolted together. The material of the modules is low carbon steel.

## III. DIPOLE MAGNET

A very limited axial domain of 2 m was allocated for the large aperture 2 $\mathrm{T}\cdot\mathrm{m}$ Dipole Magnet of the PANDA Forward Spectrometer (Fig. 1). The main flux direction in the gap is vertical and perpendicular to the beam axis.

The general concept of the dipole magnet is based on an "H" form return yoke, fabricated from low carbon steel sheets. The flat horizontal pole tips follow the defined acceptance angle of 10°. The dipole coils have an unusual saddle shape without straight parts. The coils are wound from a hollow aluminum conductor 50 mm $\times$ 50 mm cooled by circulating de-mineralized water. The maximum temperature rise of the cooling water is 30°C. The main parameters of the magnet are given in Table IV.

TABLE IV
MAIN PARAMETERS OF THE DIPOLE MAGNET

| | |
|---|---|
| Ampere-turns of the DM winding, A | $6.6\cdot10^5$ |
| Average current density, A/m$^2$ | $1.5\cdot10^6$ |
| Field integral in the aperture, T·m | 2.05±0.08 |
| Maximum flux density at the beam axis, T | 0.85 |
| Power consumption, kW | 446 |
| Winding Current, A | 4230 |
| Weight of Al conductor, kN | 105 |
| Weight of the Iron Yoke, kN | 2240 |
| Subcoil turn average lengths, m | 10.5/11.2/11.8 |

The winding consists of two identical coils. Every coil includes three subcoils supported by clamps enveloping the coils via rubber gaskets.

The iron yoke consists of six parts: bottom and top blocks, two uprights and two pole pieces. All parts consist of separate modules, which are rigidly connected by means of bolts, slotted flanges and tie rods.

The dipole magnet is attracted to the neighboring solenoid with a force of 4 kN. The average value of the field integrals along straight lines inside the rectangular conical aperture equals $2.05 \pm 0.08\ \mathrm{T}\cdot\mathrm{m}$.

## IV. CONCLUSION

Conceptual design of the PANDA magnet system has been developed. The absence of the requirement of radiation transparency for the coil materials allows us to make the solenoid coil design different from the traditional design of large detector solenoids with aluminum stabilized coil implying an inner winding method. Thus the operational current of the solenoid and consequently the cost of the solenoid maintenance can be reduced.

The Dipole Magnet design with a very short axial length was developed in accordance with the strict space limitation.

## REFERENCES

[1] PANDA Conceptual Design Report: An International Accelerator Facility for Beams of Ions and Antiprotons. [Online]. Available: http://www.gsi.de/GSI-Future/cdr

[2] A. Herve *et al.*, "Status of the construction of the CMS (compact Muon spectrometer) magnet," in *Proc. 18th Intern. Conf. on Magnet Technology (MT-18)*, 2002, vol. 14, p. 548, no. 2.

[3] A. B. Oliva *et al.*, "Zeus magnet construction status report," in *Proc. 11th Intern. Conf. on Magnet technology (MT-11)*, Tsukuba, 1989, p. 201.

[4] M. Larin, T. Mormose, H. Ishimary, and N. Gotoh, "Liquid helium cryopumps with low-emissivity Al film coating and low helium consumption," *Journal of Vacuum Science and Technology A. Second Series*, vol. 13, no. 5, pp. 2579–2581, Sept./Oct. 1995.

[5] HTS-110 Ltd: The CryoSaver Family of Current Leads. [Online]. Available: http://www.hts-110.com/products/current-leads.html